Supplementary Information for "Reaction of Trimethylaluminum with Water on Pt(111) and Pd(111) from 10^{-5} to 10^{-1} Millibar"

Michael D. Detwiler,[†] Amir Gharachorlou,[†] Lukas Mayr,[‡,§] Xiang-Kui Gu,[†] Bin Liu,[‖] Jeffrey Greeley,[†] W. Nicholas Delgass,[†] Fabio H. Ribeiro,[†] Dmitry Y. Zemlyanov[§]*

†School of Chemical Engineering, Purdue University, West Lafayette 47907, United States

‡Institute for Physical Chemistry, University of Innsbruck, A-6020 Innsbruck, Austria

‖Department of Chemical Engineering, Kansas State University, Manhattan 66506, United States

§Birck Nanotechnology Center, Purdue University, West Lafayette 47907, United States

1. XPS Coverage and Thickness Model Derivations

Differential photoelectron peak intensity as a function of photoemission angle, $I_s(\theta)$, from a bounded, uniform density substrate, *s*, can be written as:

$$I_s(\theta) = I \times \rho \times \frac{d\sigma_s}{d\Omega} \times \Omega(\theta, \varphi) \times \varepsilon \times \exp\left(\frac{-z}{\Lambda_s(E_s) \times \cos\theta}\right) dz \quad (1.1)$$

where I is the x-ray flux, and is constant in most spectrometer systems at constant hν; Ω is the acceptance solid angle of the electron analyzer; ε is the instrument detection efficiency, which is the probability that an escaped electron encompassed by the acceptance solid angle will yield a single count; ρ is the number of atoms or molecules per unit volume, $\frac{d\sigma_s}{d\Omega}$ is differential cross-section for the substrate photoemission peak, which can be calculated from Scofield cross sections[1] and the Reilman asymmetry parameter,[2] and $\Lambda_s^{E_s}$ is the electron attenuation length of an electron originating from the substrate which was calculated using NIST SRD-82,[3] θ is the

angle of electron takeoff relative to the surface normal. The exponential term is the probability for no-loss escape from the specimen, where $\frac{z}{\cos\theta}$ is the path length.

Integrating,

$$\int I_s(z) = \int_{-\infty}^{\infty}\int_{-\infty}^{\infty}\int_{0}^{\infty} I \times \rho \times \frac{d\sigma}{d\Omega} \times \Omega(x,y,z) \times \exp\left(\frac{-z}{\lambda_s(E_s)\cos\theta}\right) \quad (1.2)$$

$$I_s(\infty) = I \times \Omega(\theta) \times A(\theta) \times \varepsilon \times \rho \times \frac{d\sigma}{d\Omega} \times \lambda(\theta) \times \frac{S}{S} \times \frac{d\Omega}{4\pi} \quad (1.3)$$

where A_s is the effective substrate area.

2. Derivation of model for coverage calculation assuming a semi-infinite substrate and a non-attenuating overlayer at fractional monolayer coverage

This derivation follows the approach by Fadley.[4]

Substrate peak intensity, $I_s(\infty)$, for a semi-infinite substrate, where the substrate is represented by subscript *s*, can be represented by Equation 2.1, where the limit of Equation 1.3 is taken as t

tends to infinity:

$$I_s(\infty) = N_s \times \Omega_s(E_s) \times \sigma_s(E_s) \times \varepsilon_s \times \frac{d\sigma_s}{d\Omega} \times \frac{d\Omega}{4\pi} \times \lambda_s(E_s) \times \cos\theta \quad (2.1)$$

Peak intensity from the overlayer, represented with subscript *l*, is written as:

$$I_l(\infty) = N_l \times \Omega_l(E_l) \times \sigma_l(E_l) \times \frac{d\sigma_l}{d\Omega} \times \varepsilon_l \times \frac{d\Omega}{4\pi} \quad (2.2)$$

Where N_s is the average surface density of atoms in the overlayer in cm^{-2}.

The ratio of overlayer to substrate peak intensity can be written as:

$$\frac{I_o(o)}{I_s(s)} = \frac{N_o \times \Omega_o(E_o) \times \sigma_o(E_o) \times \theta \times \lambda_o(E_o) \times \cos\theta}{N_s \times \Omega_s(E_s) \times \sigma_s(E_s) \times \lambda_s(E_s) \times \cos\theta} \quad (2.3)$$

Where $d_o = N_o/N_s$ d_o is the average separation of layers of density N_s in the substrate. Solving

for N_o/N_s then yields the coverage:

$$\frac{N_o}{N_s} = \frac{I_o(o) \times N_s \times \Omega_s(E_s) \times \sigma_s(E_s) \times \lambda_s(E_s) \times \cos\theta}{I_s(s) \times \Omega_o(E_o) \times \sigma_o(E_o) \times \lambda_o(E_o) \times \cos\theta} \quad (2.4)$$

For the case of the *in situ* XPS experiments, $\Omega_o(E_o) \approx \Omega_s(E_s)$ and $\sigma_o(E_o) \approx \sigma_s(E_s)$ for constant pass energies, and $\theta = 0°$, so Equation 2.4 simplifies to:

$$\frac{N_o}{N_s} = \frac{I_o(o) \times \lambda_s(E_s)}{I_s(s) \times \lambda_o(E_o)} \quad (2.5)$$

For UHV-XPS experiments, $\lambda_o(E_o) \approx \lambda_s(E_s)$, and $\lambda_s = d_o$ for constant pass energies so Equation 2.5

simplifies to:

$$\frac{N_o}{N_s} = \frac{I_o(o) \times \Omega_o(E_o) \times \sigma_s(E_s) \times \lambda_s(E_s) \times \cos\theta}{I_s(s) \times \Omega_o(E_o) \times \sigma_o(E_o) \times d_o} \quad (2.6)$$

3. Derivation of model for thickness, *t*, of uniform overlayer, l, on top of substrate s

Peak intensity of the overlayer, $I_l(E_l)$, follows directly from equation (1.2), integrating over z from 0 to *t*:

$$I(E) = \times \Omega(\theta) \times A(\theta) \times n \times \rho \times \frac{E_l}{E} \times \Lambda(\theta) \times \cos\theta \times \Omega \times \left(1 - \exp\left(\frac{-t}{\lambda_l(E_l) \times \cos\theta}\right)\right) \quad (3.1)$$

Where $\lambda_l(E_l)$ is the electron attenuation length of an electron originating from the overlayer with

kinetic energy E_l through the overlayer.

For the substrate, equation 1.2 is integrated over z from *t* to infinity in the case of a semi-infinite substrate, yielding:

$$I(E) = \times \Omega(\theta) \times A(\theta) \times n \times \rho \times \frac{E_s}{E} \times \Lambda(\theta) \times \cos\theta \times \Omega \times \left(\exp\left(\frac{-t}{\lambda_s(E_s) \times \cos\theta}\right)\right) \quad (3.2)$$

Where $\lambda_s(E_s)$ is the electron attenuation length of an electron originating from the substrate with

kinetic energy *Es* through the overlayer.

Rearranging, solving for t, and cancelling similar terms yields the following:

3. Derivation of model for thickness, *t*, of uniform overlayer deposited on top of substrate s

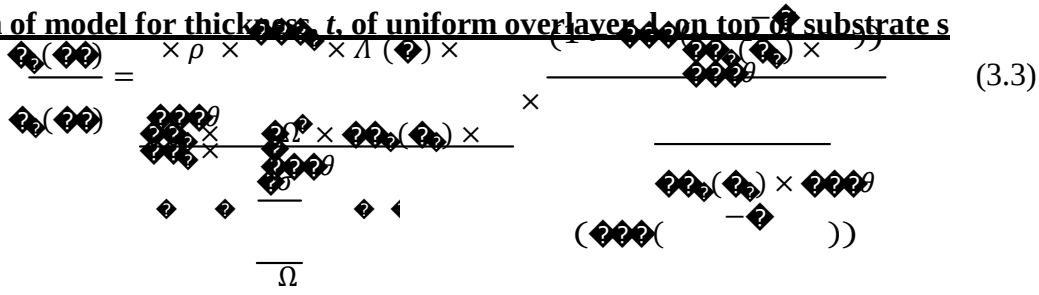

(3.3)

For the *in situ* XPS experiments, $E_l = E_s$ due to selection of photon energy, so $\lambda_{E_l}(E_l) \approx \lambda_{E_s}(E_s)$.

For the *in situ* experiment, cosθ=1. In this case, thickness can be solved for explicitly:

$$d = \lambda_{E_s}(E_s) \times \ln\left(\frac{I(E_l) \times \rho \times \lambda_{E_l} \times \Omega}{I_0(E_l) \times \rho_0 \times \lambda_{E_s} \times \Omega_0} + 1\right) \qquad (3.4)$$

4. Derivation of carbon coverage using CO standard

Due to absorption of some of the X-ray flux by the window in the *in situ* cell between the bending magnet and chamber, quantification of the C 1s coverage as outlined above was not successful. Instead, this coverage was estimated by dosing CO in saturation (assumed to be 0.5 ML) on Pt(111),[5] and using atomic concentration ratios as outlined below to calculate the carbon coverages on Pt(111) and Pd(111).

Carbon coverage on surface *i* was estimated using equations 4.1 and 4.2, by comparison of atomic concentration *(C/Pt)* ratios between the CO saturated Pt(111) surface and the *(C/Pt)* ratio for surface *i* on Pt(111):

$$\frac{(C/Pt)_{CO/Pt(111)}}{(C/Pt)_i} = \frac{0.5\ ML}{\theta_i} \qquad (4.1)$$

$$[illegible]v[illegible]a[illegible] = 0.5\ [illegible] \frac{([illegible]/P[illegible])_i}{([illegible]/P[illegible])_{c[illegible]}} \qquad (4.2)$$

[illegible]

×

For Pd(111), carbon coverage on surface *i* was estimated in a similar manner by converting the C/Pt ratio for CO saturation to a C/Pd ratio by using the appropriate Pd relative sensitivity factor and x-ray flux values.

O 1s Regions on Pt(111)

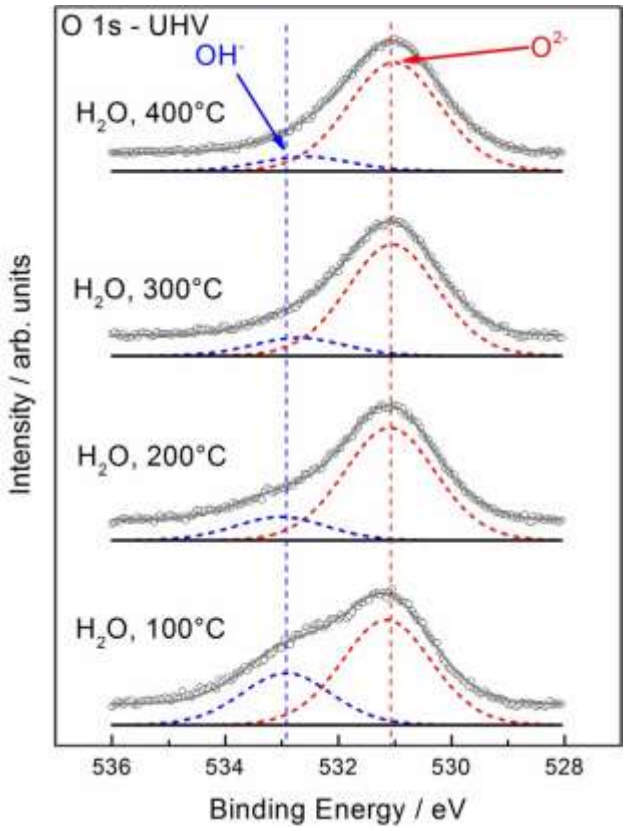

Figure SI-1. O 1s high resolution core level spectra for the UHV-XPS experiment on Pt(111). From bottom to top: After exposure to water at 100°C following TMA exposure and subsequently in steps to 400°C. Fitted components are shown as dashed lines and represent O^{2-} bound to Al (red) and OH^- bound to Al (blue). The open circles are raw data points, and the light grey line is the sum of the deconvoluted peaks.

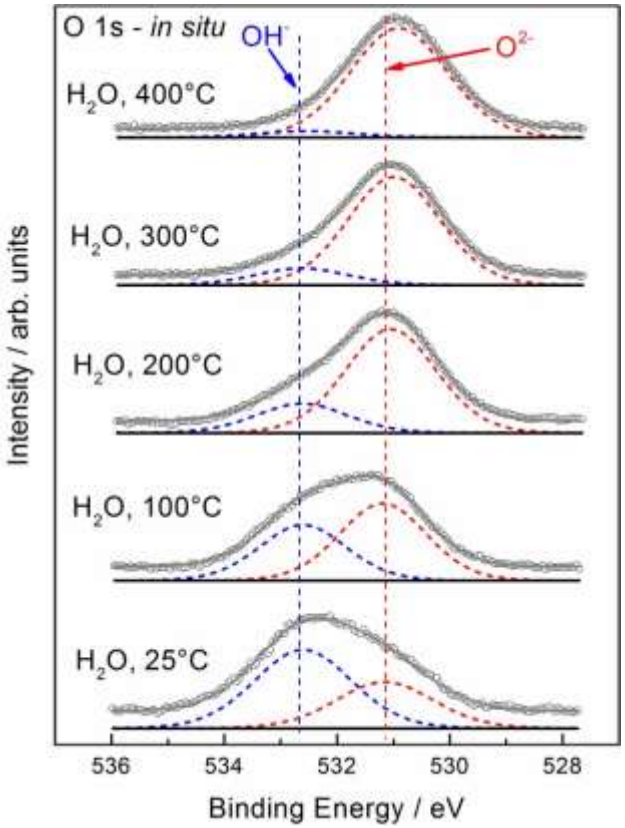

Figure SI-2. O 1s high resolution core level spectra for the *in situ* experiment on Pt(111). From bottom to top: Pt(111) single crystal after exposure to water at 25°C following dosing of TMA and subsequently in steps to 400°C. Fitted components are shown as dashed lines and represent O^{2-} bound to Al (red) and OH^{-} bound to Al (blue). The open circles are raw data points, and the light grey line is the sum of the deconvoluted peaks.

Calcination Experiment on Pd(111)

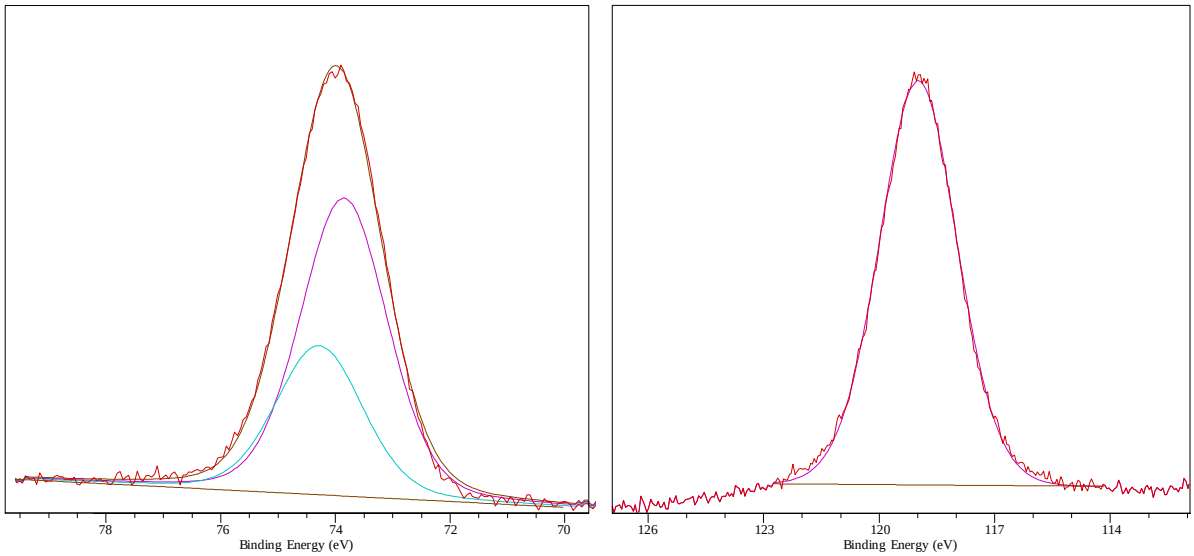

Figure SI-3. Shown above are the Al 2p (left) and Al 2s (right) regions following the calcination experiment described in the body of the text. The Al $2p_{3/2}$ peak is located at 74.0 eV (Al $2p_{1/2}$ also shown at 74.4 eV), and the Al 2s peak is located at 119.0 eV.

C 1s Core Level Region from Pd(111) in H_2O, 400°C (*in situ* XPS)

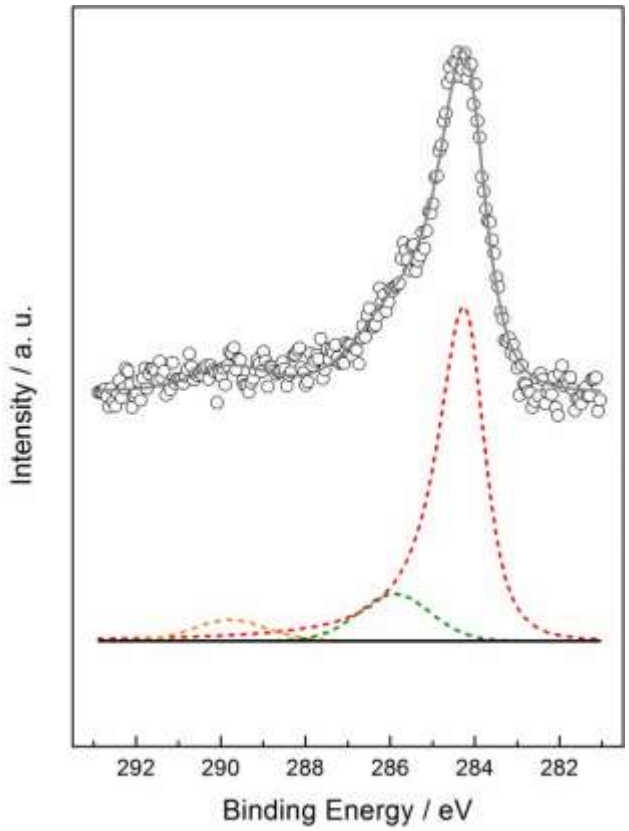

Figure SI-4.

C1s high resolution core level region for *in situ* XPS on Pd(111) during exposure to 0.1 mbar water at 400°C. Fitted components originating from carbon-containing components are shown as orange (adsorbed carboxyl), dark green (adsorbed CO), and red (assignment discussed in text) dashed lines. The open circles are raw data points, and the light grey line is the sum of the deconvoluted peaks.

Discussion on Alumina Crystallization

Several studies involving high resolution XPS have investigated various aluminum oxide/hydroxide phases and stoichiometries on surfaces. Mulligan et al.[6] studied aluminum oxide films formed on NiAl(110) following oxidation using synchrotron radiation XPS. Oxygen adsorption at 300 K resulted in 3 new states on a metallic surface: chemisorbed oxygen at 74.26-74.53 eV, tetrahedral amorphous-like alumina at 75.93, and octahedral Al^{3+} at 76.81 eV (only observed at exposures greater than 51 L). After 1200 L exposure of oxygen at 300 K, the resulting layer contains 90% tetrahedral aluminum. The authors attribute this to amorphous alumina, which is the only bulk phase composed of mainly tetrahedral alumina. Absolute and relative amounts of octahedral aluminum increase after annealing at 573 and 1073 K. The authors attribute this to migration of subsurface Al to the oxidized layer. This increase in octahedral aluminum results in an increase in the highest BE peak at 76.81 eV. The layer formed at 1073 K is γ-alumina-like based on the relative amounts of octahedral and tetrahedral aluminum. The authors base their assignments on the works of Bianconi et al.[7] and McConville et al.[8] who used high resolution XPS to study the Al 2p core level. Bianconi et al. combined Al 2p XPS with X-ray absorption near-edge spectroscopy (XANES) data and observed metallic Al at 73.0 eV, shifts of 1.4 eV for chemisorbed O and 2.8 and 3.3 eV for oxide states. The chemisorbed state at +1.4 eV was observed at room temperature along with the metallic state. The oxide state at +2.8 eV was observed after annealing to 200°C, and the state at +3.3 eV was observed after annealing to 400°C. McConville et al. observed shifts of +0.49 ± 0.02 (chemisorbed state 1) State 2, +0.97 ± 0.03 State 3, 1.46 Oxide state, 2.5-2.7 eV. The shift to higher BE for more ordered alumina overlayers was confirmed also by Kovács et al.[9] who assigned Al 2p peaks at 74.2 and 74.9 to amorphous Al_2O_3 and γ- or α-alumina, respectively.

All of the above references show a shift to higher binding energy for more crystalline alumina, but we observed a shift to lower BE while heating in water. Therefore, this binding energy shift is likely not caused by the transition from tetrahedral to octahedral Al_2O_3.

REFERENCES

1. Scofield, J. H., Hartree-Slater Subshell Photoionization Cross-Sections at 1254 and 1487 eV. *J. Electron. Spectrosc. Relat. Phenom.* **1976**, *8*, 129-137.

2. Yeh, J.; Lindau, I., Atomic Subshell Photoionization Cross Sections and Asymmetry Parameters: 1⩽< I> Z</I>⩽ 103. *At. Data Nucl. Data Tables* **1985**, *32*, 1-155.

3. Powell, C. J.; Jablonski, A., *NIST Electron Effective-Attenuation-Length Database - Version 1.3*; National Institute of Standards and Technology: Gaithersburg, MD, 2011.

4. Fadley, C. S., Basic Concepts of X-Ray Photoelectron Spectroscopy. In *Electron Spectroscopy: Theory, Techniques and Applications*, Brundel, C. R.; Baker, A. D., Eds. Academic Press: New York, 1978; Vol. 2.

5. Ertl, G.; Neumann, M.; Streit, K. M., Chemisorption of CO on Pt(111) Surface. *Surf. Sci.* **1977**, *64*, 393-410.

6. Mulligan, A.; Dhanak, V.; Kadodwala, M., A High-Resolution Photoemission Study of Nanoscale Aluminum Oxide Films on NiAl(110). *Langmuir* **2005**, *21*, 8312-8318.

7. Bianconi, A.; Bachrach, R. Z.; Hagstrom, S. B. M.; Flodstrom, S. A., Al-Al_2O_3 Interface Study Using Surface Soft-X-Ray Absorption and Photoemission Spectroscopy. *Phys. Rev. B* **1979**, *19*, 2837-2843.

8. Mcconville, C. F.; Seymour, D. L.; Woodruff, D. P.; Bao, S., Synchrotron Radiation Core Level Photoemission Investigation of the Initial-Stages of Oxidation of Al(111). *Surf. Sci.* **1987**, *188*, 1-14.

9. Kovacs, K.; Perczel, I. V.; Josepovits, V. K.; Kiss, G.; Reti, F.; Deak, P., In Situ Surface Analytical Investigation of the Thermal Oxidation of Ti-Al Intermetallics up to 1000 °C. *Appl. Surf. Sci.* **2002**, *200*, 185-195.